AMERICAN METEOROLOGICAL SOCIETY

Journal of Applied Meteorology and Climatology

The DOI for this manuscript is doi: 10.1175/2009JAMC2230.1

Southeast Pacific Stratocumulus: High Frequency Variability and Meso-scale Structures over San Félix Island

David Painemal

Rosenstiel School of Marine and Atmospheric Sciences, University of Miami

René Garreaud, José Rutllant

Department of Geophysics, Universidad de Chile

Paquita Zuidema

Rosenstiel School of Marine and Atmospheric Sciences, University of Miami

Corresponding author address: David Painemal, RSMAS/MPO, University of Miami, 4600 Rickenbacker Causeway, Miami, FL 33149-1098.
E-mail: dpainemal@rsmas.miami.edu

Abstract

Stratocumulus cloud cover patterns and their relationship to drizzle were characterized at San Felix Island (SFI: 26.5°S, 80°W) in the Southeast Pacific. Small closed, large closed and open cells were identified in about 65% of the MODIS (Moderate Resolution Imaging Spectro-radiometer) satellite images during 2003. The MODIS imagery was combined with ceilometer and surface meteorological measurements, human observations of cloud types and drizzle, and large-scale meteorological analyses for January through June. We identified two drizzle regimes: a synoptically-quiescent summer (Jan-March) regime characterized by a strong anticyclone, large closed cells, and frequent drizzle, and an autumn (April-June) regime characterized by a weaker anticyclone, small closed cells and open cells, and precipitation that was mainly associated with synoptic activity. The large closed cells had higher mean cloud bases and tops than the small closed cells, accounted for 45% of the cumulus-under- stratocumulus reports, and 29% of the total drizzle and rain reports. Large closed cells occupied more intermittently-coupled boundary layers than did the small closed cells. Open cells also occurred in more decoupled conditions, but only accounted for 18% of the total reports of drizzle and rain. The atmospheric stability of large and small closed cells were similar, but large closed cells were more commonly associated with a strong anticyclone, and small closed cells with wave activity superimposed upon a weakened anticyclone. The increased drizzle and occurrence of cumulus-under-stratocumulus in the summer rather than autumn is consistent with higher nighttime liquid water paths. A contribution of this study is the documentation of the ways in which synoptic activity can affect stratocumulus decks.

1. Introduction

Interest in subtropical warm clouds (namely stratus and stratocumulus (Sc)) arises from their importance to the earth's radiative budget (Hartmann et al.1992) and the need for the cloud's accurate representation in global climate models (e.g. Kiehl and Gent 2004; Wittenberg et al. 2006). The Southeastern Pacific (SEP) stratocumulus deck, under the quasi-permanent influence of the southeast Pacific anticyclone, is arguably the most persistent of the planet's decks (Fig. 1). Geographical seasonal variability in the stratocumulus deck cloud cover is nevertheless high. The largest development of the Sc deck over SEP is observed in JJA (Fig. 1c) and SON (Fig. 1d), with the deck primarily located off the coast of Peru. In contrast, during austral summer, the highest cloud cover occurs off of the central-northern Chilean (20˚S-30˚S) coast (Fig. 1a), when the anticyclone center reaches its most poleward location.

Detailed satellite imagery of the stratus cloud decks shows the striking spatial patterns of meso-scale convection cells (MCC, e.g., Bretherton et al., 2004; Agee, 1973; Garay et al., 2004). These cells can be schematically characterized by well defined hexagons with diameters between 10 and 100 km. Depending on the clear/cloudy condition in the center of the cell, such cells are classified as open/closed cell structures (a detailed review of mesoscale cellular convection can be found in Atkinson and Zhang (1996)). Their characterization encompasses satellite studies (e.g., Wood and Hartmann, 2006; Jensen et al., 2008; Wood et al. 2008) and more detailed but small-sample-size case studies (Stevens et al., 2005; Comstock et al., 2005; Sharon et al., 2006). Both Wood and Hartmann (2006) and Jensen et al. (2008) found that closed cells with larger cell diameters typically possess higher liquid water paths and occupy deeper boundary layers,

than closed cells with smaller diameters. Wood and Hartmann (2006), in their examination of Sep-Oct 2000 data, found a lack of sensitivity of their cellular patterns to the large-scale meteorological conditions (i.e. lower-tropospheric stability, surface temperature advection, and 850-hPa vertical velocity), speculating that internal boundary layer mechanisms were important for the transition from closed to open cells. Jensen et al. (2008) also considered effective radius as a drizzle proxy and sampled a much longer time period than Wood and Hartmann (2006). They identified two seasonally-varying drizzle regimes for the SEP stratus region, a trait that distinguished the SEP region from other stratocumulus decks. One goal for this current study is to reconcile the findings of Wood and Hartmann (2006) and Jensen et al. (2008) for this region, and one question addressed is if MCC sampled over a longer time period may yet be preferentially associated with particular large-scale meteorological conditions.

Satellite-only studies cannot easily probe the interior of the boundary layer, and few studies have simultaneously characterized the boundary layer structure underlying mesoscale cellular cloud structures systematically identified using satellite imagery, along with their large-scale meteorological conditions, for a significant period of time. During January-June of 2003 a laser ceilometer and an automatic weather station (AWS) were operated at San Felix Island (SFI: 26º16'S, 80º05'W). Though a modest deployment, it provided a unique opportunity to characterize stratocumulus cellular cloud patterns from both surface and space for a longer period than documented in previous studies (e.g., Comstock et al., 2005; Petters et al. 2006; Wood et al., 2008). San Felix Island is located slightly south (and upwind) of the region selected by Klein and Hartmann (1993) for their characterization of SEP stratus, and is in the southeastern

corner of the SEP region studied by Wood et al. (2006). SFI is located well away from the continent (~ 850 km off the coast of north-central Chile), is small (total area of 2.5 km^2), possesses modest orography (maximum height of 193m a.s.l.) and has good exposure to the southeastern trade winds. The January-June time frame coincided with the SEP deck's most dramatic seasonal change (Fig.1), suggesting the full range of stratocumulus cloud variations could be sampled. The island's location also complements studies based on buoy-tending ship cruise data typically gathered further north and of shorter time durations (e.g., Garreaud et al. 2001, Kollias et al., 2004; Serpetzoglou et al. 2008; Wood et al., 2008).

Datasets and methods are described in Section 2, Section 3 presents analyses of the surface-based measurements, Section 4 discusses the satellite-derived cellular structures, while Section 5 contains concluding remarks.

2. Data and methods

A Campbell Scientific AWS was installed on the windward southeastern coast of SFI (50 m above sea level, a.s.l.) in December 2002, and recorded 30-min averages of air temperature and relative humidity, wind speed and direction, atmospheric pressure, solar and net radiation and precipitation thereafter (Table 1). A CT12K Vaisala laser ceilometer, either similar to or the same as the one used during the First International Satellite Cloud Climatology Project (ISCCP) Regional Experiment (pers. comm. Bruce Albrecht, see Albrecht et al. (1990)), was also installed at that time, until June 2003. The ceilometer retrieved the lowest –first– cloud base height~~s~~ occurring every 30 sec up to 12500 feet (3810 m) with 50 feet (15.24 m) of vertical resolution. The ceilometer data

were used to estimate both an hourly-mean cloud base height and the standard deviation of the cloud base height about the hourly mean. An hourly cloud frequency (CF) was defined as the ratio between the number of cloud-base returns below 2300 m (the highest cloud base observed over SFI) a.s.l. and the total number of measurements (120) in the corresponding hour. During February and most of March 2003 nighttime measurements (1-5 LST) were not performed due to electric power restrictions. Diurnal cycle results for large closed cells mostly rely on data collected during January, and may be slightly biased as a result.

Hourly sea-surface temperatures (SST_{bulk}, a bulk measurement collected 2 meters below sea level from a tide-gage station) and 3-hour weather observations of drizzle and cloud types were also routinely reported by the Chilean Navy at SFI. The low-cloud classification along with the associated synoptic code can be found in Norris (1998). At SFI, the dominant cloud types were: Sc (Sc not resulting from the spreading out of cumulus Sc, code 5) and Cumulus-under-Sc (code 8). These cloud types together accounted for 78.2% and 40% of the total reports in January to March (JFM) and April to June (AMJ) respectively (Table 2). In this study closer attention is paid to the Cu-under-Sc type in an effort to relate cloud type to decoupling and precipitation. Cu-under-Sc was more commonly reported, and Sc less so, at SFI during 2003 than at the more-studied Weathership N at 30˚N, 140˚W (Klein et al. 1995, Klein 1997; Norris, 1998).

A drizzle event was simply defined as light rain not necessarily recorded by the rain gauge but reported by the human observer. The lifting condensation level (LCL) was estimated following Lawrence (2005) after first combining the SST_{bulk} and the specific humidity from the AWS to establish the relative humidity over the ocean. This assumed

that the cloud bases at the windward side of the island respond more to conditions over the ocean than over the island. The LCL value derived this way was insensitive to diurnal variations in the island air temperature. An unknown remained the air-sea temperature difference; the air temperature is typically less than the SST_{bulk} by about 1˚C, but this can vary with the season (Zuidema et al., 2009; Serpetzoglou et al., 2008). A constant (negative) offset of 150 m was applied to the LCL to account for the air-sea temperature difference, determined by matching the LCL to the cloud base height on days 95-105 (see Fig. 3b), a period with low and less variable cloud base heights and LCLs, and cloud base heights that track well with each other, indicating a well-coupled boundary layer. Similar offsets were determined for other selected time periods. The offset is equivalent to an air-SST_{bulk} difference of ~ 1.2˚C.

NCEP/NCAR Reanalysis (Kalnay et al., 1996) was used to determine the regional circulation over SFI. In particular, a lower tropospheric stability (LTS, Klein and Hartmann, 1993) was calculated as the difference between potential temperature at 700 hPa and 1000 hPa from the Reanalysis.

A satellite-derived cloud top height (CTH) was also incorporated to estimate the depth of the boundary layer. This was obtained by combining the cloud top temperature (CTT) from MODIS (Moderate Resolution Imaging Spectro-radiometer; level 2 product, Collection 5, 5 km horizontal resolution, on both AQUA and TERRA satellites with each satellite passing over the region twice per day), with the 3-day-mean sea surface temperature from the Tropical Rainfall Measuring Mission Microwave Imager (SST_{TMI}), following Zuidema et al., (2009). In that study, a linear relationship (eq. 1) was derived based on the inversion base height (reported by 156 collocated radiosondes launched in 6

cruises within the SEP region) and CTT-SST_{TMI} differences, and valid for cloud tops between 800 to 2000 m.

$$CTH = \frac{SST_{TMI} - CTT - 2.35}{0.0069} \quad [\text{m}] \quad 800<\text{CTH}<2000 \text{ m} \qquad (1)$$

Overpass CTHs were then combined to form a daily-mean cloud top height estimate. In general, the estimates of cloud top height trended well with cloud base height (also supporting our assumption that the mean cloud base heights were not overly affected by drizzle and cloud vertical structure). The daily mean CTH was obviously underestimated on days 24 and 124 (Fig. 3), when CTH < CBH. On day 24 eqn (1) was extended beyond its lower limit of 800 m, while day 124 may reflect a thin cloud not meeting the assumption of blackbody infrared emissivity.

Cellular mesoscale structures above SFI were defined from the MODIS-Terra satellite visible-only radiances (level 1 product, with a spatial resolution of 1 km^2 and local satellite overpass time at approximately 11 am) over a 250 km by 250 km area. These provided coverage for the full year of 2003, allowing investigation of the entire seasonal cycle and providing context for the ceilometer data. Visual inspection, a suitable and accurate technique for this dataset size, was used to classify the cloud structures into four groups. Small and large closed-cell structures were defined by cell diameters (λ) of < 30 km and > 30 km respectively. These were also calculated using 2D Fourier transform (typical cell diameter was defined as $\lambda = (\lambda_x^2+\lambda_y^2)^{1/2}$ with λ_x and λ_y the zonal and meridional wavelength) by selecting the λ with the peak in the spectrum. The third group consisted of open-cell structures, while the fourth group included all structures that did not clearly fit into the previously defined categories. The open-cell structures were not necessarily examples of the pockets of open cells described by Stevens et al. (2005)

or Wood et al. (2008), as they were not necessarily embedded within a larger region of closed cells. Examples of each category are shown in Fig. 2.

Liquid water path data from a microwave satellite-derived diurnal climatology covering 1988-2007, described further in O'Dell et al. (2008), also complemented the SFI analysis. A unique feature of this climatology is an explicit diurnal cycle derived by combining data from a number of microwave satellites with different equatorial overpass times. We rely on the climatology rather than using 2003-only values because of the climatology's insight into the diurnal cycle, which is aided by the averaging done over many years. Monthly-mean values for 2003 were close to the climatological values.

3. Results

3.1 Time Series

Time series of measured cloud base heights (CBH), LCL, CTH, and LTS are depicted in Fig. 3, along with indicators for the observer reports of drizzle and cloud types, and AWS-detected rain. A general inspection of Fig. 3 indicates that both CTH (black filled circles) and CBH vary together at synoptic scales. Cumulus-under-stratocumulus was the most frequently reported cloud type (Table 2). Reports of drizzle (black open circles) and light rain (crosses) were more frequent during JFM (Fig. 3a) than AMJ (Fig. 3b). Additionally, Cu-under-Sc (blue open circles in the lower panel of Figs. 3a and b) was reported more frequently during JFM (56% of the observations, Fig. 3a, lower panel), than AMJ (27% of observations, Fig. 3b, lower panel).

The entire time-series mean CTH of 1408 m yields a mean cloud depth of 352 m. The mean CTH value agrees well with the mean inversion height from radiosondes

launched near SFI during the October 1999 CIMAR-6 cruise (Garreaud et al. 2001), which gave an overall inversion height of about 1500 m.

A closer look at the daily values of CF and LTS (Fig. 4) anticipates a positive correlation between LTS (Fig. 4 gray line) and CF (Fig. 4 black line), though CF varies at shorter time scales than LTS. Values for the linear correlation between LTS and morning mean values (6-9 LST, time frame chosen to avoid nighttime data gaps) of CF and CBH were similar: 0.4 and -0.41 respectively. These coefficients increased to 0.7 when daily values were low-passed with a 20-day cut-off *Butterworth* filter. The cloud top heights also correlated well with lower tropospheric stability (r= -0.38 using daily mean values). The high CBH-LTS correlation can be understood as a tendency for cloud bases to move up and down with the cloud tops at synoptic time scales. Given that LTS-CF correlations can vary regionally (e.g., Stevens et al., 2007), it is of interest that the LTS-CF correlation values at SFI are fairly similar to those at the weathership N in the northeast Pacific (Klein 1997).

During April-June (Fig. 3b), periods with precipitation reports were less common and associated with less variable CBHs (e.g. days 95 to 105 and 120 to 125). At times, the cloud base and LCL were nearly the same (e.g., day 95-105; used to establish the initial LCL offset), indicating a well-coupled boundary layer. More periods with a drastic decrease in LTS and reduced cloud cover are apparent (e.g. day 105-115, Fig. 4). Perusal of satellite imagery and meteorological analyses during the austral fall revealed that overcast episodes of 3-5 days preceded the passage of mid-tropospheric ridge axes that warmed the air aloft, raising the LTS. Conversely, clear-sky episodes were observed ahead of eastward-moving 500 hPa trough axes (decreasing LTS). Cumulonimbus were

more common (23.3%) during April-June (table 2) and associated with incoming synoptic troughs.

The seasonal changes described above can be connected with changes in both drizzle (and light rain) and boundary layer coupling. During austral summer (January-March) drizzle events did not seem to correlate well to the atmospheric stability (black line, lower panel in Fig. 3a). Drizzle was also observed when the cloud base was well above the LCL (e.g., day 70-75), which should indicate decoupling. In contrast, during the austral fall (April-June), light rain/drizzle was observed when lower LTS reflected enhanced mid-latitude synoptic wave activity. Stated more quantitatively, the LTS deviations-from-the-mean associated with rain/drizzle were -0.2˚C and -1.2˚C during summer and fall, respectively. Similarly, the deviations-from-the-mean associated with no drizzle/rain were 0.23 and 0.31 for summer and fall respectively.

The relationship between boundary layer coupling and cloud base height variability is addressed more explicitly in Fig. 5, where the difference between the daily-mean CBH and LCL (the degree of boundary layer coupling), and the daily standard deviation of the CBH (only for CF> 0.2) are depicted in the scatterplot. The cases with reported precipitation (filled circles in Fig. 5) show an enhanced CBH standard deviation along with a higher CBH-LCL difference. Additionally, the days with high standard deviation and CBH-LCL differences are concurrent with cases of Cu-under-Sc (crosses in Fig. 5). Most of the drizzle cases are also associated with this Cu-Sc configuration. Indeed, the presence of Cu penetrating the stratocumulus cloud deck is associated with drizzle in 44% of the cases. Thus, high-frequency CBH variability reflects both drizzle,

which can artificially register a lower cloud base, and Cu-under-Sc, which truly yield highly variable cloud bases.

These differences in the relationship between drizzle, CTH, CBH and the atmospheric stability for January-March versus April-June suggest two distinctive boundary layer regimes: a summer regime with regular drizzle, frequent cumulus-under-stratocumulus, and less variable atmospheric stability, and an autumn regime with less precipitation and larger variations in atmospheric stability and cloud fraction.

3.2 Diurnal Cycle

The diurnal cycle in cloud properties for January and May (Fig. 6) further distinguishes the processes characterizing the two seasonal time periods. January-mean LCLs were 400 m lower than those for May, possibly reflecting an overall moister summertime boundary layer. Similarly, January nighttime-mean CBHs of ~1050 m were ~150 m less than those of May. In both months the mean LCL was well below the CBH. A strong diurnal cycle in cloud frequency was evident for January (Fig. 6a), with cloudy conditions during nighttime (mean CF>0.6), reducing during the morning to usually clear-sky afternoon conditions (mean CF<0.3). The diurnal cycle in cloud frequency was consistent with the 1988-2007 climatological fitted satellite-derived liquid water path (LWP) diurnal cycle. Climatological-mean nighttime LWP values in January almost reach 110 g m^{-2}, for which light precipitation is common (e.g., Zuidema et al., 2005), helping to explain the frequent reports of light precipitation in January. Similarly, the nighttime build up of liquid water is consistent with intermittently-coupled conditions,

with moisture entering the cloud through the Cu penetrating the Sc deck reported by the human observers.

A slight diurnal cycle in both CBH and LCL can be seen for January (Fig. 6b). A rising cloud base during the afternoon can be seen more expressly for a few individual days (day 6 and 8, better seen in Fig. 11c; note that 20 GMT ~ 15 LST). This is consistent with afternoon cloud shortwave absorption that encourages decoupling of the cloud layer turbulent circulation from the subcloud turbulent circulation, reducing the moisture flux to the cloud, and contributing to the pronounced January diurnal cycle in cloud frequency.

Numerical simulations (Fig. 5 of Garreaud and Muñoz (2004)) indicate the presence of a broad diurnal maximum in the free-tropospheric subsidence at SFI between 0700-1500 LST (approximately -1 cm/s, Fig. 5 of Garreaud and Muñoz, 2004). This feature, attributable to the heating of Andes Cordillera, is also evident in an October CTH climatology (Fig. 10 of Zuidema et al. (2009)). We found that the amplitude of CTH diurnal cycle observed at SFI (Fig. 6b, 90 m and 80m for summer and spring respectively), while not statistically significant, did suggest some modulation of the free-tropospheric subsidence, reflected in a CTH minimum at 14 LST.

During May the cloud frequency remained nearly constant during the day, consistent with only a slight diurnal cycle in the climatological LWP. The diurnal cycle during May for CBH and LCL was also fairly uniform (Fig. 6b), at about 1200 m and 650 m respectively. While the diurnal-mean LWP values were similar for May as for January, the diurnal maximum value of ~ 70 g m^{-2} is not typically associated with precipitation, consistent with a more synoptic origin for any observed precipitation.

For both months, the diurnal cycle of the air temperature (Fig. 6c) reaches its maximum at 15 LST. That the maximum air temperature during May is not followed by a change in cloud frequency supports the assumption that island heating contributes little to the observed CF diurnal cycle.

4. Cellular patterns

Thus far we have described the evolution of the boundary layer over SFI along with changes in precipitation and the coupling/decoupling of the boundary layer. The next step is relating these changes to the stratocumulus mesoscale structures. Annual 2003 occurrence statistics for each cell structure category are given in Table 3, while Fig. 7 presents the time series for the occurrence of the structures. Cellular patterns occurred more than half of the time (65.3%) in all of the images combined, especially open cells (27.3%), with closed cells, both small and large, totaling 38%. The highest occurrence of large closed-cell structures was found in austral spring and summer (75% of all images from October-March), while the small closed cells occurred mostly in austral fall and winter (81% of all images from April-September). Open-cell structures could be found in all seasons, but tended to concentrate in austral fall and winter (68% of all images from April-September). Statistically, slightly more open cells and fewer closed cells were documented at SFI's location than by Wood and Hartmann (2006) for September and October of 2000.

Fig. 8 illustrates the differences in CTH and degree of boundary layer coupling among cellular patterns. Large closed cell clouds (gray squares) are present within more decoupled boundary layers with higher CTHs, while the small closed cells (black

diamonds) are associated with more coupled boundary layer with lower CTHs. The mean large and small closed-cell heights of ~1600 and ~1350 m exceed those reported by Wood and Hartmann (2006; Fig. 17) for the characteristic cell length scales (~40 and ~20 km), thought to reflect the different MODIS Collections and equations used to estimate CTH within the two studies (see Zuidema et al., 2009). Fig. 8 also suggests that deeper boundary layers (higher CTH) are more likely to be decoupled (r = 0.42 associated with Fig. 8, when CTH lower than 1000 m are discarded)

The mean diurnal cycle of the large closed-cells (Fig. 9) has remarkable amplitude in CF, while for small closed cells the diurnal cycle is modest. Both closed-cells structures have a diurnally-constant CBH (Fig. 9b) though it is more than 200 m higher for large closed-cells. The diurnal cycle of LCL confirms that large closed-cells tend to be more decoupled than the small closed-cells. Open cells are also characterized by decoupled conditions (Fig. 9b), primarily because they have the lowest mean LCL, with few reports of drizzle or rain (only 18% of the total). The diurnal cycle in CF for open cells also shows a significant amplitude but with reduced mean CF.

Mean values of the cloud base and top heights, cloud base height standard deviation, and height difference between the cloud base and lifting condensation level for each cell pattern are given in Table 4. We found daily standard deviations of 176 m and 124 m for the large and small closed cells group respectively, consistent with Cu-under-Sc being more prevalent during the large-closed cells episodes. In fact, 45% of the Cu-under-Sc reports and the 29% of the drizzle (or rain) reports occurred on days with large closed cells. Open cells had the highest CBH standard deviation (253 m) and also the smallest cloud coverage (table 4). Lower tropospheric stability values were similar for the

large- and small closed cells (20.0 and 19.8 ^{0}C respectively), exceeding those for the open cells (18.4 ^{0}C), consistent with the positive correlation between cloud fraction and LTS. The higher standard deviation in LTS and CBH for open cells indicates that they can be observed over a broad range of conditions: in fact 23% (17%) of the open cases occurred before or after a large (small) closed cell event.

The breakdown of cloud property statistics by the cellular pattern helps explain an apparent discrepancy in Fig. 6, where the January-mean cloud base height is seen to lie below the May-mean cloud base height, despite the greater occurrence of large closed cells in January, which have higher cloud bases (Table 4), and of small closed cells in May, which have lower cloud bases. The key fact is that both months also contain time periods with open cells, which have highly variable cloud base heights. In January, open-cells had a low CBH (days 20-25), while in May they featured high cloud bases (days 130-138). Therefore these open-cell cloud bases ended up contributing strongly to the mean CBH for each month.

We now illustrate with the composite fields of sea level pressure (SLP) and 500 hPa geopotential height for each cellular group. In addition, we include the analysis of typical cases. The selected cases correspond to the time periods indicated by gray bars on Fig. 7.

4.1 Large closed cell

The mean SLP and 500 hPa geopotential fields for the composite of large closed cell patterns (Fig. 10) are characterized by a strong anticyclone (contours) with no significant development of waves at 500 hPa (shades), typical conditions that prevail in austral summer. The first week of January 2003 was a typical example, featuring a

persistent closed cellular pattern over SFI with cell lengths larger than 40 km (Fig. 11). Precipitation was occasionally recorded by the SFI rain-gauge (Fig. 3a). Frequent ceilometer vertical traces (and high CBH variability) suggested the presence of cumulus growing into the upper stratocumulus cloud and/or drizzle. The SLP pattern (Fig. 12) shows a strong anticyclone with its center at 40˚S, without much mid-tropospheric activity in terms of wave patterns.

4.2 Small closed cell

A weak anticyclone and a ridge axis to the southwest of SFI are the mean conditions for the composite of the small closed cell group (Fig 13), a pattern likely to occur in austral fall and winter. The typical case observed in April (Fig. 14) presented similar features as the group composite (Fig. 13): the CBHs were steady and very close to the LCL, indicative of a high degree of coupling within the MBL. AWS records indicated only one precipitation event within this 10 day period (Fig. 3b), without accompanying downward traces in the ceilometer return signals. Consistent with the composite fields, the surface anticyclone (Fig. 15) was weaker than the large closed-cell example, but this time was accompanied by a well-developed geopotential wave pattern at 500 hPa with a ridge axis at 95˚S. Such a pattern will induce subsidence to the east of the ridge at the location of the SFI (note also the clearing southeast of SFI in Fig. 14).

4.3 Open-cell typical case

The SLP composite (Fig. 16) for all of the open-cell cases has a similar pattern to the small closed cell SLP, but now the otherwise-smooth structure at 500 hPa suggests

a weak trough over SFI (a ridge west of SFI). Though well-defined cases of open cells were more common during austral winter (June-August), some open-cell-like structures were also observed during May. During the days 130-138 (May 10-18), a few open cell structures along with light-rain episodes were detected around SFI. The atmospheric stability decreased significantly during this time period, the sky cleared, and the CBH was highly variable (Fig. 3a). On day 135 (May 15) clear skies were embedded within a broader region with open-cell-like structures, while on day 137 (May 17) an open cell was observed near SFI, shown in Fig. 17. The meteorological analysis connected changes in the anticyclone with a well-developed eastward-moving trough at 500 hPa (Fig. 18). These conditions induce cold advection above the boundary layer and ascent over the SFI region. This period was a distinctive example of precipitation associated with mid-latitude weather disturbances.

In some images, a pocket of open cells (Stevens et al. 2005) or rift (Sharon et al. 2006) could be identified; these were typically classified as open-cell structures. No distinctive meteorological features were observed for these more localized pockets of open cells. A significant proportion (~30%) of the images were also classified as lacking any particular cellular pattern. This may reflect a limitation to using only a 250 x250 km^2 area to classify each image, with some of the "no cellular pattern" cases in fact embedded within larger structures. The large-scale meteorological fields associated with this group were not systematically analyzed, but short-lived significant weather disturbances may plausibly have a strong influence on this category.

5. Concluding Remarks

We have studied the Sc variability over SFI (26º16'S, 80º05'W) with a combination of 6 months (January to June 2003) of surface-based ceilometer data, automatic weather station records and human synoptic reports, and one year (2003) of visible MODIS satellite imagery. Our analysis suggests two characteristic regimes of cloud morphology and drizzle over SFI:

- A synoptically-quiescent summer regime (January-March) characterized by a strong subtropical anticyclone, large closed cells, and frequent drizzle. Cumulus-under-stratocumulus was the most common surface-observed cloud type during summer months.
- A fall regime (April-June) characterized by a weakened anticyclone, small closed and open cells, and episodes of light precipitation associated with passage of synoptic disturbances.

We venture that these two regimes provide an explanation to the two drizzle regimes found by Jensen et al. (2008): one synoptically-driven and occurring more frequently during the austral fall, and the other driven by nocturnal buildup of liquid water. Consistent with Jensen et al. (2008), who used MODIS-derived effective radius as a drizzle proxy, we find using observer reports that drizzle is more frequent in large closed cells than small closed cells. Consistent with Jensen et al. (2008) and Wood and Hartmann (2006), we also find that large closed cells are deeper and have higher cloud tops and bases. An arguably more unique observational contribution of this study is that large closed cells are also more intermittently-coupled than small closed cells, as indicated by larger differences between their CBH and LCL.

Since no apparent large-scale meteorological feature explains the summer drizzle, it is thought to result from a more local collision-coalescence process. This process becomes active when condensation has produced larger "collector" drops, for which larger cloud liquid water paths can serve as a proxy. Cumulus rising from below into the Sc cloud deck serves as one source of moisture condensation for the larger drops. Though not shown here, this may be aided at night by both a less stable cloud-subcloud layer, and a less stable capping of the surface mixed layer (Klein et al. 1995). Cumulus-under-stratocumulus clouds were more commonly observed during JFM and generally associated with large closed cells. During the Atlantic Stratocumulus Transition Experiment (ASTEX), Bretherton and Pincus (1995), while not explicitly categorizing their cases according to mesoscale cellular cell length, sampled Cu-under-Sc cases reminiscent of such large closed cells. In one closed cell case, Miller and Albrecht (1995) found that major drizzle events corresponded to a deepening of the cumulus layer, with cumulus transporting surface moisture to the upper cloud layer, similar to what our data suggest for large closed cells. The higher cloud bases and greater decoupling for the larger closed cells should also encourage light drizzle to evaporate before reaching the surface, allowing a recycling of the water vapor back into the cloud (e.g., Comstock et al. 2005). The ASTEX observations also suggested that above-inversion humidity variations could impact cloud structure, an issue we have not investigated within this study.

Monthly-mean LWP values did not decrease much between January and May (Fig. 6), but the diurnal cycle weakened considerably, with maximum nighttime values below 80 g m^{-2} by May, reducing the ability of the collision-coalescence process to produce drizzle. The diurnal cycle in cloud frequency was also much more pronounced in January

than in May. A high January nighttime cloud frequency occurred despite a 500 m difference between the LCL and CBH for large closed cells, but is consistent with intermittent coupling by cumulus rising into stratocumulus. The January afternoon minimum in CF is attributed to shortwave absorption.

The bulk stability of the lower troposphere (LTS) explained about 50% of the variance in CF, CTH, and CBH after the high-frequency variability was removed, similar to that computed by Klein (1997) for weathership N in the northeast Pacific. Beyond this statistical result, examination of daily weather maps suggests that large closed cells are more commonly associated with a strong anticyclone, while the small closed cells are associated with subsidence from mid-latitude wave activity superimposed upon weaker anticyclones. This larger-scale view of the regional circulation distinguishes this study from that of Wood and Hartmann (2006), who did not find a sensitivity of the cell size to selected large-scale meteorological variables. No characteristic time sequences in the size of closed-cell cloud patterns were seen. However, about 40% of the closed-cell patterns occurred before or after open-cell ones, as continuous overcast and clear-sky periods over broad areas around SFI were closely related with mid-latitude ridges and troughs, respectively.

In contrast to this study, Wood and Hartmann (2006) found that open cells tended to occupy deeper boundary layers than closed cells, while this study found open cells occupy boundary layers of variable depth. These differences can reflect the different regional focus and different time lengths sampled, with the open cells of Wood and Hartmann (2006) typifying the equatorward stratocumulus to trade-wind cumulus transition, while the open cells categorized here come from an entire year and are more

influenced by mid-latitude synoptic intrusions into the southeast Pacific stratocumulus region. While this may reflect SFI's position at the southern edge of the main stratocumulus deck as defined by Klein and Hartmann (1993), Xu et al. (2005) also documented a significant synoptic contribution to the overall variability in cloud properties at 20˚S, 85˚W in their longer-term study.

We speculate that large-closed structures can be expected in austral summer when the storm tracks and associated mid-troposphere waves of the westerlies are shifted poleward. The greater likelihood of large closed cells during summer and small closed cells during winter may arise from differences in SST. The large closed cells, being more decoupled than the small closed cells, rely more on rising thermals driven by the warmer SSTs to sustain them.

ACKNOWLEDGMENTS: We are indebted to Prof. Bruce Albrecht from the U. of Miami for making us available the ceilometer. The maintenance of the ceilometer and the automatic meteorological station at San Felix Island was carefully accomplished by meteorologists of the Chilean Navy. We would also like to thank all personnel from the Chilean Navy at Valparaiso (I Naval Zone and Hydrographic and Oceanographic Services) and those stationed at San Felix Island for their collaboration, including transportation to and from the Island. We gratefully thank Chris O'Dell for supplying the satellite liquid water path data used within the diurnal cycle Fig. 6, which greatly aided our interpretation of that figure. Grants from FONDECYT Project 1020833 and the University of Chile support through its Department of Geophysics and the Multidisciplinary Program for Atmospheric and Climate Dynamics (PRODAC) from the

Department of Research contributed to fund this activity. Support from the NOAA Climate Prediction Program of the Americas award NA06OAR4310056 for DP and PZ is gratefully acknowledged. We thank Robert Wood and two other anonymous reviewers for their careful reading of the manuscript.

References

Agee, E. M., T. S. Chen, K. E. Dowell, 1973: A review of mesoscale cellular convection. *Bull. of Amer. Meteor. Soc.*, 54, 1004-1012.

Albrecht, B.A., C.W. Fairall, D.W. Thomson, A.B. White, J.B. Snider, and W.H. Schubert, 1990: Surface-based remote sensing of the observed and the adiabatic liquid water content of stratocumulus clouds. Geophys. Res. Lett., 17, 89-92.

Atkinson, B. W., and J. W. Zhang, 1996: Mesoscale shallow convection in the atmosphere. *Rev. Geophys.*, 34, 403–431.

Bretherton, C.S. and R. Pincus, 1995: Cloudiness and marine boundary layer dynamics in the ASTEX Lagrangian experiments. Part I: Synoptic setting and vertical structure. J. Atmos. Sci., 52, 2707-2723.

Bretherton, C. S., T. Uttal, C. Fairall, S. Yuter, R. Weller, D. Baumgardner, K. Comstock, R. Wood, G. Raga, 2004: The EPIC 2001 stratocumulus study. *Bull. of Amer. Meteor. Soc.*, 85, 967-977.

Comstock, K. K., C. S. Bretherton, and S. E. Yuter, 2005: Mesoscale variability and drizzle in southeast Pacific stratocumulus. *J. Atmos. Sci.,* 62, 3792-3807.

Garay, M. J., R. Davies, C. Averill and J. A. Westphal, 2004: Actinoform clouds: Overlooked examples of self-organization at the mesoscale. *Bull. of Amer. Meteor. Soc.*, 85, 1585-1594.

Garreaud, R., J. Rutllant, J. Quintana, J. Carrasco y P. Minnis, 2002: CIMAR-5: A snapshot of the lower troposphere over the subtropical southeast Pacific. *Bull. of Amer. Meteor. Soc.*, 82, 2193-2220.

Garreaud, R., R. Muñoz, 2004: The diurnal cycle in circulation and cloudiness over subtropical southeast Pacific: a modelling study. *J. Climate*, 17, 1699-1710.

Hartmann, D. L., M. E. Ockert-Bell, and M. L. Michelsen, 1992: The effect of cloud type on Earth's balance: Global analysis. *J. Climate*, 5, 1281-1304.

Jensen, M. P., A. M. Vogelmann, W. D. Collins, G. J. Zhang, and E. P. Luke, 2008: Investigation of regional and seasonal variations in marine boundary layer cloud properties from MODIS observations. *J. Climate,* 21, 670-685.

Kalnay, E. and coauthors 1996: The NCEP/NCAR 40-years Reanalysis project. *Bull. of Amer. Meteor. Soc.*, 77, 437-471.

Kiehl, J. T. and P. R. Gent, 2004: The Community Climate System Model, Version 2. *J. Climate*, 17, 3666-3682.

Klein, S. A., D. L. Hartmann, 1993: The seasonal cycle of low stratiform clouds. *J. Climate*, 6, 1587-1606.

Klein S. A., D. L. Hartmann, and J. R. Norris, 1995: On the relationships among low-cloud structure, sea surface temperature, and atmospheric circulation in the summertime northeast Pacific. *J. Climate*, 8, 1140–1155

Klein, S. A. 1997: Synoptic variability of low-cloud properties and meteorological parameters in the subtropical trade wind boundary layer. *J. Climate*, 10, 2018-2039.

Kollias, P., C. Fairall, P. Zuidema, J. Tomlinson, and G. Wick, 2004: Observations of Marine Stratocumulus in SE Pacific during the PACS 2003 cruise. *Geophys. Res. Lett*., 31 doi:10.1029/2004GL020751.

Lawrence, M., 2005: The relationship between relative humidity and the dewpoint temperature in moist air: A simple conversion and applications. *Bull. Am. Meteor. Soc.,* 86, pp. 225-233.

Mechoso, C. R., A. W. Robertson, N. Barth, M. K. Davey, P. Delecluse, P. R. Gent, S. Ineson, B. Kirtman, M. Latif, H. Le Treut, T. Nagai, J. D. Neelin, S. G. H. Philander, J.

Miller M. A., and B. A. Albrecht, 1995: Surface-based observations of mesoscale cumulus–stratocumulus interaction during ASTEX. *J. Atmos. Sci.*, 52, 2809–282.

Norris, J. R., 1998: Low cloud type over the ocean from surface observations. Part I: relationship to surface meteorology and the vertical distribution of temperature and moisture. *J. Climate*, 11, 369-382.

O'Dell, C. W., F. J. Wentz, and R. Bennartz, 2008: Cloud liquid water path from satellite-based passive microwave observations: A new climatology over the global oceans, *J. Climate.*, *21*, 1721–1739.

Petters M. D., J. R. Snider, B. Stevens, G. Vali, I. Faloona, L. Russell, 2006: Accumulation mode aerosol, pockets of open cells, and particle nucleation in the remote subtropical Pacific marine boundary layer, *J. Geophys. Res.*, 111, D02206, doi:10.1029/2004JD005694.

Rossow W. B. and E. N. Dueñas, 2004: The International Satellite Cloud Climatology Project (ISCCP) Web Site: An Online Resource for Research. *Bull. of Amer. Meteor. Soc.*, 85, 167–172.

Serpetzoglou E., B. A. Albrecht, P. Kollias and C. Fairall, 2008. Boundary layer, cloud, and drizzle variability in the southeast Pacific stratocumulus regime. *J. Climate*, 21, 6191-6214.

Sharon T. M., B. A. Albrecht, H. H. Jonsson, P. Minnis, M. M. Khaiyer, T. M. van Reken, J. Seinfeld, and R. Flagan, 2006: Aerosol and cloud microphysical characteristics of rifts and gradients in maritime stratocumulus clouds. *J. Atmos. Sci.*, 63, 983–997.

Stevens B., G. Vali, K. Comstock, R. Wood, M. C. Zanten, P. Austin, C. S. Bretherton, and D. H. Lenschow, 2005: Pockets of open cells (POCs) and drizzle in marine stratocumulus. *Bull. Amer. Meteor. Soc.*, 86, 51–57.

Stevens B., A. Beljaars, S. Bordoni, C. Holloway, M. Köhler, S. Krueger, V. Savic-Jovcic, and Y. Zhang, 2007: On the structure of the lower troposphere in the summertime stratocumulus regime of the northeast Pacific. *Mon. Wea. Rev.*, 135, 985–1005.

Wittenberg A. T., Anthony Rosati, Ngar-Cheung Lau, and Jeffrey J. Ploshay, 2006: GFDL's CM2 Global Coupled Climate Models. Part III: Tropical Pacific Climate and ENSO. *J. Climate*, 19, 698-722.

Wood R., D. Hartmann, 2006: Spatial Variability of Liquid Water Path in Marine Low Cloud: The Importance of Mesoscale Cellular Convection. *J. Climate*: Vol. 19, No. 9, pp. 1748–1764.

Wood, R., K. K. Comstock, C. S. Bretherton, C. Cornish, J. Tomlinson, D. R. Collins, and C. Fairall, 2008: Open cellular structure in marine stratocumulus sheets. *J. Geophys. Res.*, 113, D12207, doi:10.1029/2007JD009371.

Xu, H. S.-P. Xie and Y. Wang, 2005: Subseasonal variability of the southeastern Pacific stratus deck. *J. Clim*., 18, p. 131-143.

Zuidema, P., E. Westwater, C. Fairall and D. Hazen, 2005: Ship-based liquid water path estimates in marine stratocumulus. *J. Geophys. Res.*, 110, D20206, doi:10.1029/2005JD00583.

Zuidema, P., D. Painemal, S. DeZoeke and C. Fairall, 2009: Stratocumulus cloud top height estimates and their climatic implications. *J. Climate*., **22**, p. 4652-4666.

List of Figures

FIG. 1. Seasonal means in warm-cloud cover (shaded) derived from ISCCP (1983-2007, D2 data, Rossow and Dueñas, 2004) and corresponding NCEP/NCAR Reanalysis (Kalnay et al., 1996) sea- level pressure means (contours) for austral a) summer (December to February), b) autumn (March to May), c) winter (June to August), and d) spring (September to November). The location of SFI is represented by the dark square.

FIG. 2. Three cellular patterns: a) small closed cells (April 28), b) open cells (July 7) c) large closed cells (January 10) and d) an example without cellular structure (August 18). The images of the cellular structure centered at SFI are 250Kmx250Km. Typical wavelengths (λ) are indicated on the right upper corner of each image.

FIG. 3. Times series for CBH (blue dots, each 30 seconds), LCL (red line) and daily-mean CTH (black circles). Human-detected drizzle and AWS-reported light rain are represented by open circles and crosses respectively. In the lower panel the black line corresponds to LTS, the red line to SST and blue open circles the Cu under Sc reports. The time series starts in January 1st, a) January to March), b) April to June. Horizontal ticks below the 0 level indicate periods with no ceilometer records.

FIG. 4: Time series for the daily mean CF (black line) and daily mean LTS (gray line). For the mean CF, we excluded the hours 1 LST to 5 LST (period of power restriction, see the text for more information).

FIG. 5. a) Scatterplot between the daily standard deviation of CBH (σ_{CBH}) and CBH-LCL. The black circles indicate events with drizzle or light rain and the crosses represent days with presence of cumulus under Sc. They are only considered events when there are at least two daily reports of drizzle or Cu under Sc.

FIG. 6. Mean diurnal cycles for January (gray) and May (black) 2003 of ceilometer-derived a) low-cloud frequency (CF) and LWP (dashed line). b) cloud-base height (CBH, solid line), lifting condensation levels (LCL, dashed lines) and CTH (dots, gray line is the diurnal cycle for January-February and the black line for May-June). c) diurnal cycle of the island temperature recorded by AWS.

FIG. 7. Time series for the occurrence of closed and open cells over SFI during 2003. Gray bars indicate the time periods corresponding to the examples shown in Figs. 11, 14, and 17.

FIG. 8. Scatterplot between daily CTH and CBH-LCL. The small-closed and large-closed cells are represented by black diamonds and gray squares respectively, whereas the open cells by asterisks. Open circles indicate no-cellular structures. Only overcast pixels were used.

FIG. 9. Mean diurnal cycles of ceilometer-derived for large closed-cells (gray), small closed-cells (black line) and open cells (triangles), 2003 a) low-cloud frequency (CF) and

LWP, b) cloud-base height (CBH, solid line) and lifting condensation levels (LCL, dashed lines).

FIG. 10: Large closed cell composite. Contours indicate SLP and shades geopotential height at 500 hPa. The thick square represents the location of SFI.

FIG. 11. An example of a period with large closed cell patterns: a) day 2 (Jan 2), b) day 6, with their correspondent enlargement around SFI (260Km by 260 Km area). The thick square represents the location of SFI. c) ceilometer cloud bases and LCL (black line) estimated from SST and moisture.

FIG. 12. Sea level pressure (contours) and geopotential height at 500 hPa (shaded) for day 2.

FIG. 13. Small closed cell composite. Contours indicate SLP and shades geopotential height at 500 hPa. The thick square represents the location of SFI.

FIG. 14. As in FIG. 11 but for a small closed cell period: a) day 98 (April 8), b) day 102 and c) ceilometer cloud bases and LCL (black line).

FIG. 15. As in FIG. 12 but for day 98.

FIG. 16. Open cell composite. Contours indicate SLP and shades geopotential height at 500 hPa. The thick square represents the location of SFI.

FIG. 17. As in FIG. 11 but for a open-cell like period: a) day 135 (May 15), b) day 137 and c) ceilometer cloud bases and LCL (black line).

FIG. 18. As in FIG. 11 but for day 136.

TABLE 1. AWS sensors

Instrument	Net radiometer	pyranometer	RH/thermometer	barometer	anemometer
Model	NR-LITE	LiCor/Li 200X-L	Vaisala / HMP35C	Vaisala / PTA427	RMY wind sentry set

TABLE 2. Cloud type occurrence (low clouds) during the period of study.

Cloud Type	**JFM [%]**	**AMJ [%]**
(1) Small Cu	4.3	0
(2) Cumulus of moderate or strong vertical extent	4.3	10
(3) Cumulonimbus (no anvil)	5.8	23.3
(4) Sc from the spreading out of Cu	5.8	3.3
(5) Sc only	21.7	13.3
(6) Stratus (St)	1.4	13.3
(7) Stratus fractus of bad weather or cumulus fractus of bad weather, or both	0	10
(8) Cu under Sc	56.5	26.7

TABLE 3. Percentage occurrence of cloud patterns from satellite imagery centered on San Felix Island during 2003.

Structure		**Ocurrence [%]**
Cellular Pattern	Open cells	27.3
	Closed cells (large)	19.5
	Closed cells (small)	18.5
Clear		5.4
Undefined patterns		29.3

TABLE 4. Daily values of CTH, CBH, CBH – LCL, the standard deviation in CBH (STD; daily), CF, LTS, and number N of contributing cases, for the 3 cellular structures. Bold values indicate statistically significant values (significant at the 95% level according to the Student's t test).

	Open cells	**Small-CC**	**Large-CC**
CTH [m]	1237±386	1347±213	**1599±256.7**
CBH [m]	997±224	944±117	**1185±178.8**
CBH – LCL [m]	562±145	**208±118**	535±145
STD [m]	**253±95.5**	**124±56.4**	**176±60.13**
CF	**0.4±0.2**	**0.55±0.19**	**0.68±0.24**
LTS [˚C]	**18.4±2.6**	20±1.76	19.8±1.94
N	82	55	58

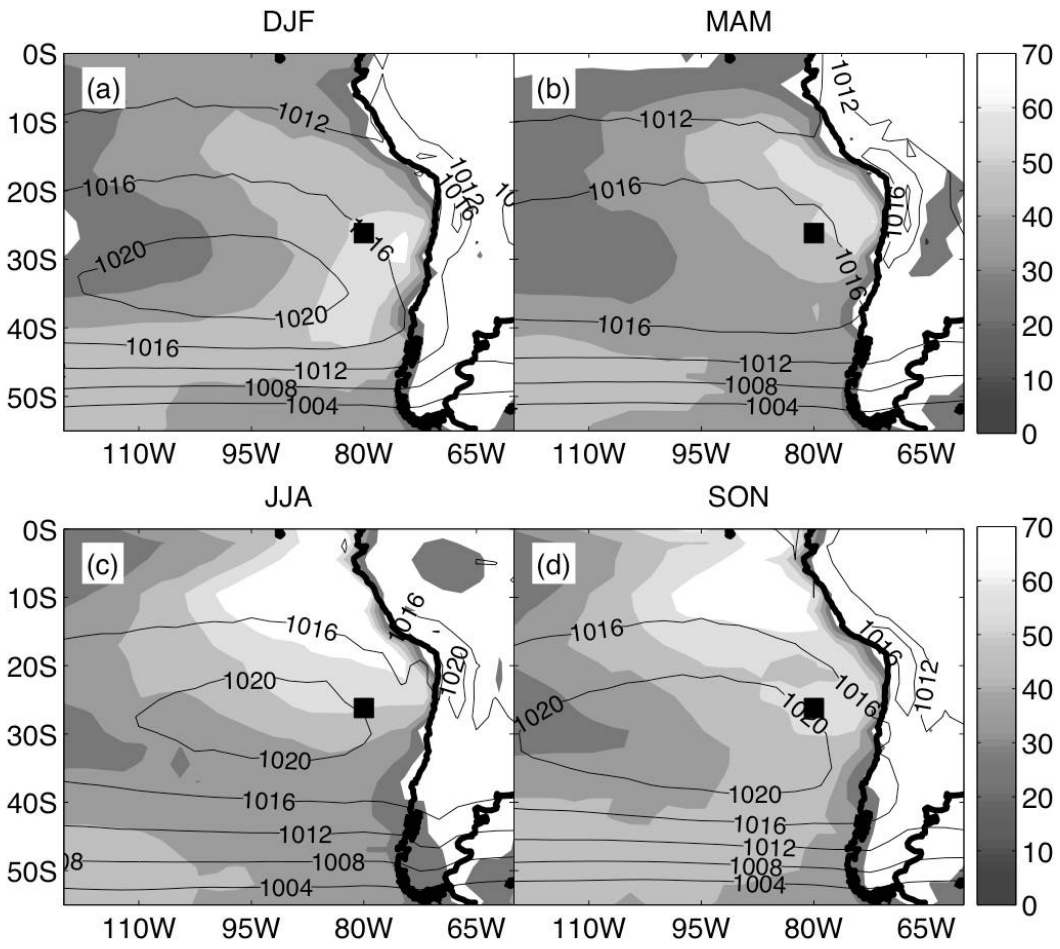

FIG. 1. Seasonal means in warm-cloud cover (shaded) derived from ISCCP (1983-2007, D2 data, Rossow and Dueñas, 2004) and corresponding NCEP/NCAR Reanalysis (Kalnay et al., 1996) sea- level pressure means (contours) for austral a) summer (December to February), b) autumn (March to May), c) winter (June to August), and d) spring (September to November). The location of SFI is represented by the dark square.

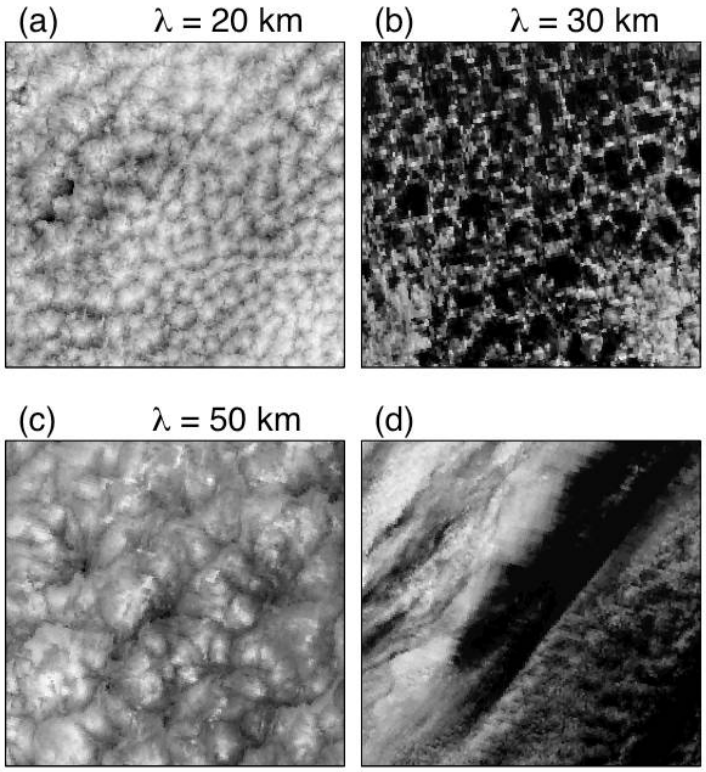

FIG. 2. Three cellular patterns: a) small closed cells (April 28), b) open cells (July 7) c) large closed cells (January 10) and d) an example without cellular structure (August 18). The images of the cellular structure centered at SFI are 250Kmx250Km. Typical wavelengths (λ) are indicated on the right upper corner of each image.

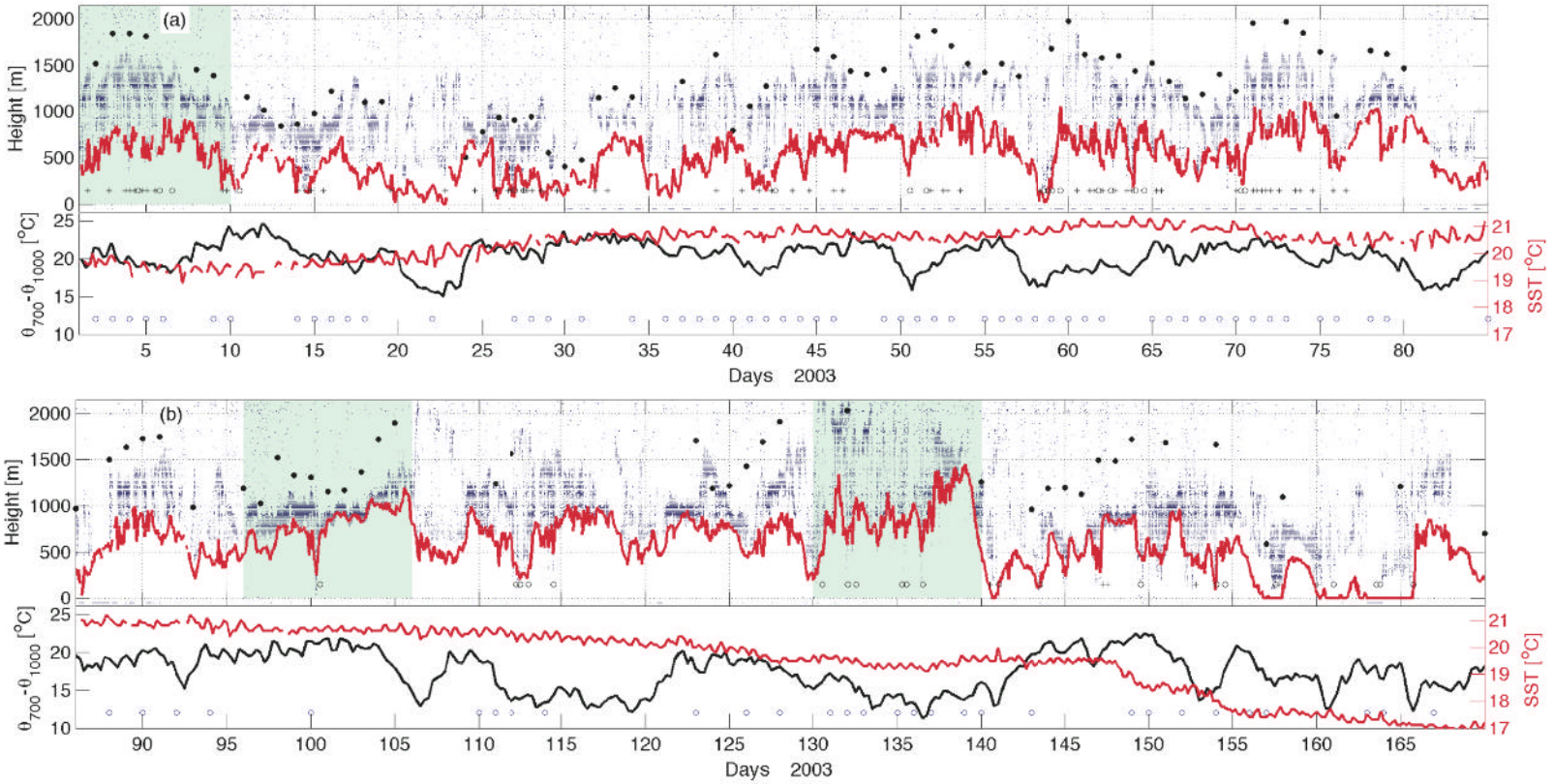

FIG. 3. Times series for CBH (blue dots, each 30 seconds), LCL (red line) and daily-mean CTH (black circles). Human-detected drizzle and AWS-reported light rain are represented by open circles and crosses respectively. In the lowerpanel the black line corresponds to LTS, the red line to SST and blue open circles the Cu-under-Sc reports. The time series starts in January 1st, a) January to March), b) April to June. Horizontal ticks below the 0 level indicate periods with no ceilometer records.

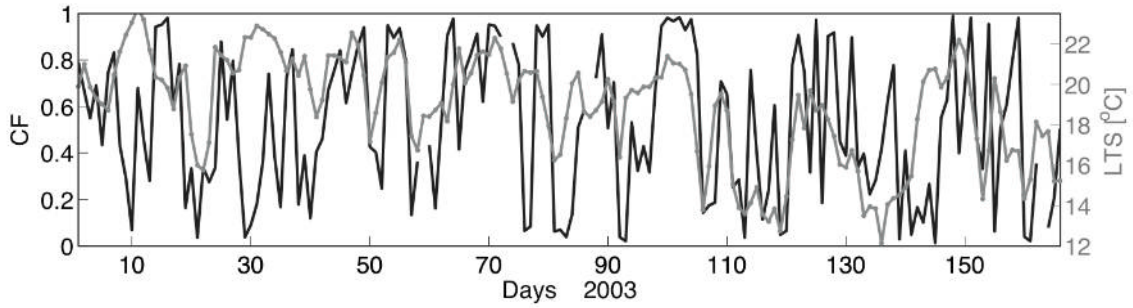

FIG. 4: Time series for the daily mean CF (black line) and daily mean LTS (gray line). For the mean CF, we excluded the hours 1 LST to 5 LST (period of power restriction, see the text for more information).

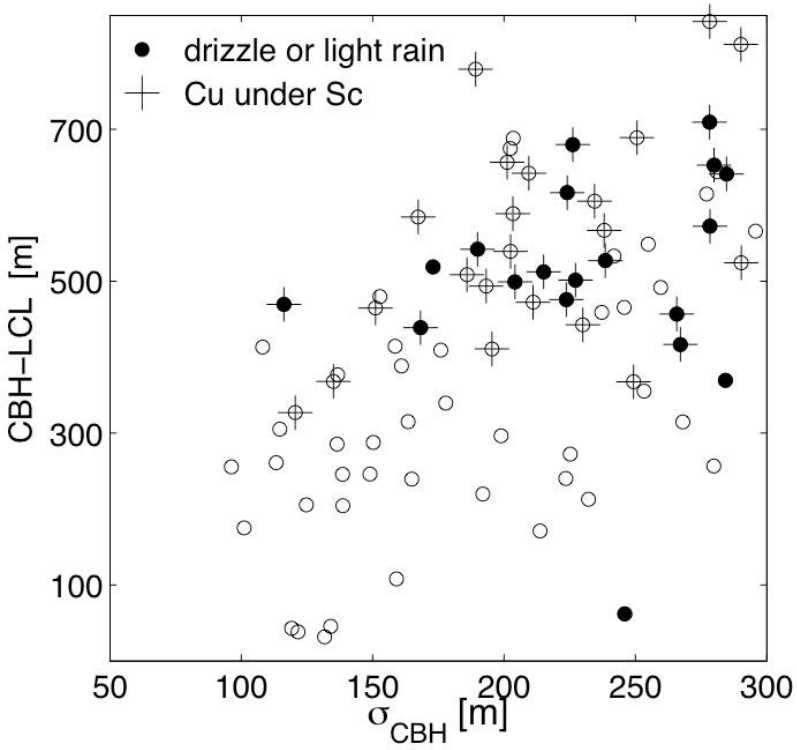

FIG. 5. a) Scatterplot between the daily standard deviation of CBH (σ_{CBH}) and CBH-LCL. The black circles indicate events with drizzle or light rain and the crosses represent days with presence of cumulus under Sc. They are only considered events when there are at least two daily reports of drizzle or Cu under Sc.

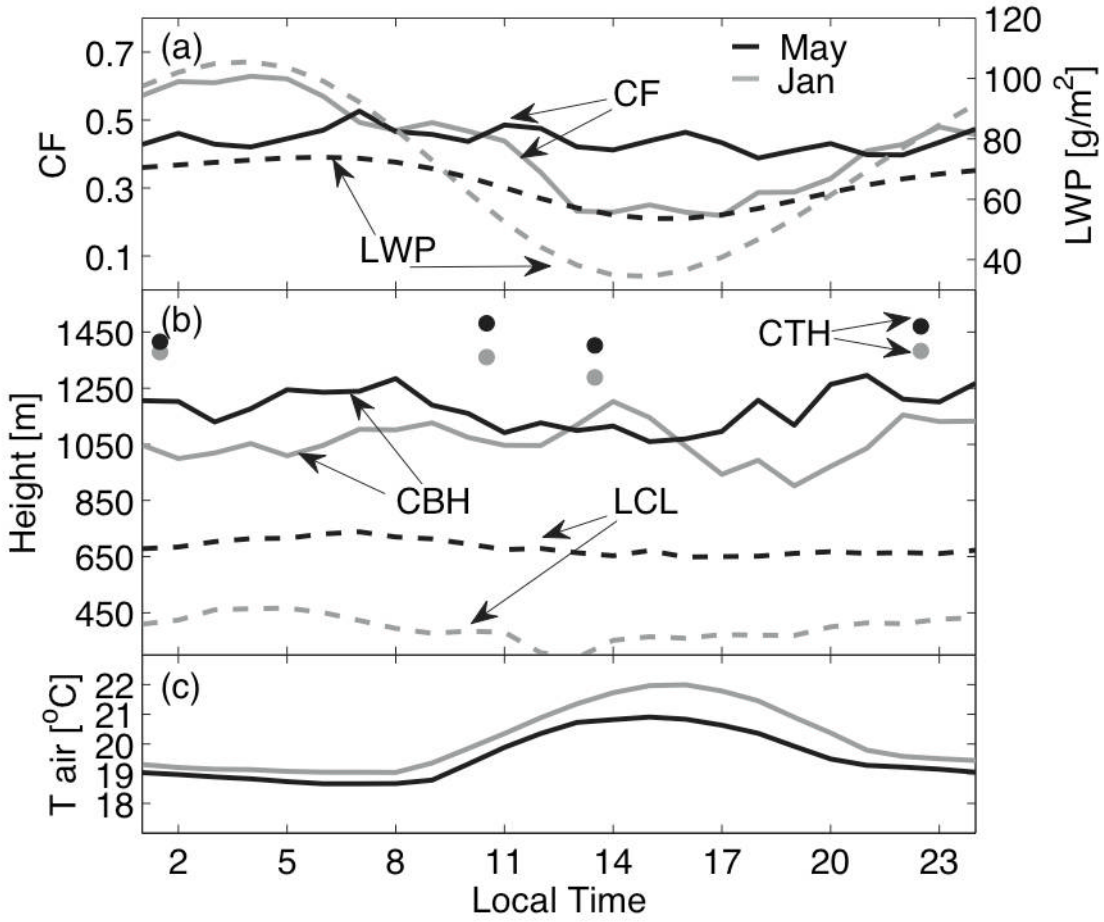

FIG. 6. Mean diurnal cycles for January (gray) and May (black) 2003 of ceilometer-derived a) low-cloud frequency (CF) and LWP (dashed line). b) cloud-base height (CBH, solid line), lifting condensation levels (LCL, dashed lines) and CTH (dots, gray line is the diurnal cycle for January-February and the black line for May-June). c) diurnal cycle of the island temperature recorded by AWS.

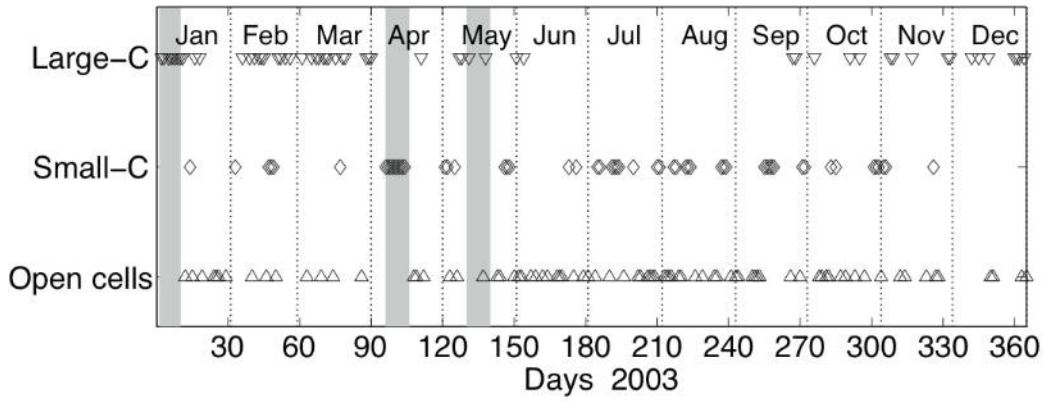

FIG. 7. Time series for the occurrence of closed and open cells over SFI during 2003. Gray bars indicate the time periods corresponding to the examples shown in Figs. 11, 14, and 17.

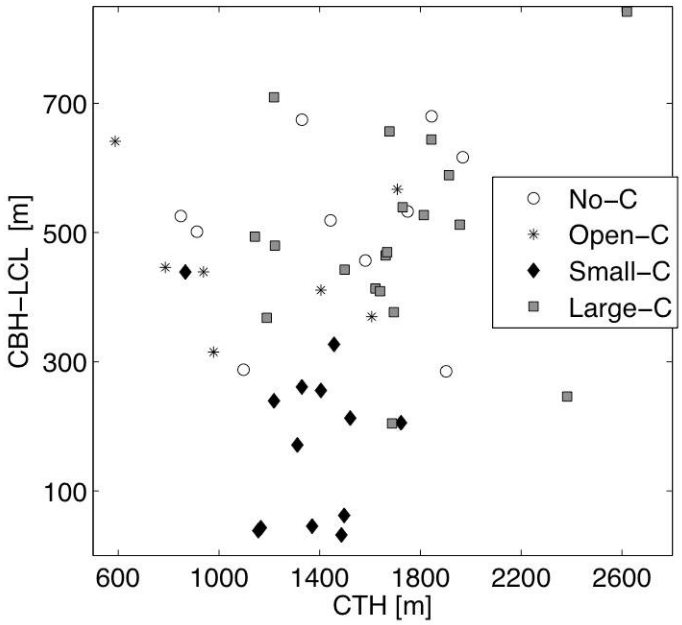

FIG. 8. Scatterplot between daily CTH and CBH-LCL. The small-closed and large-closed cells are represented by black diamonds and gray squares respectively, whereas the open cells by asterisks. Open circles indicate no-cellular structures. Only overcast pixels were used.

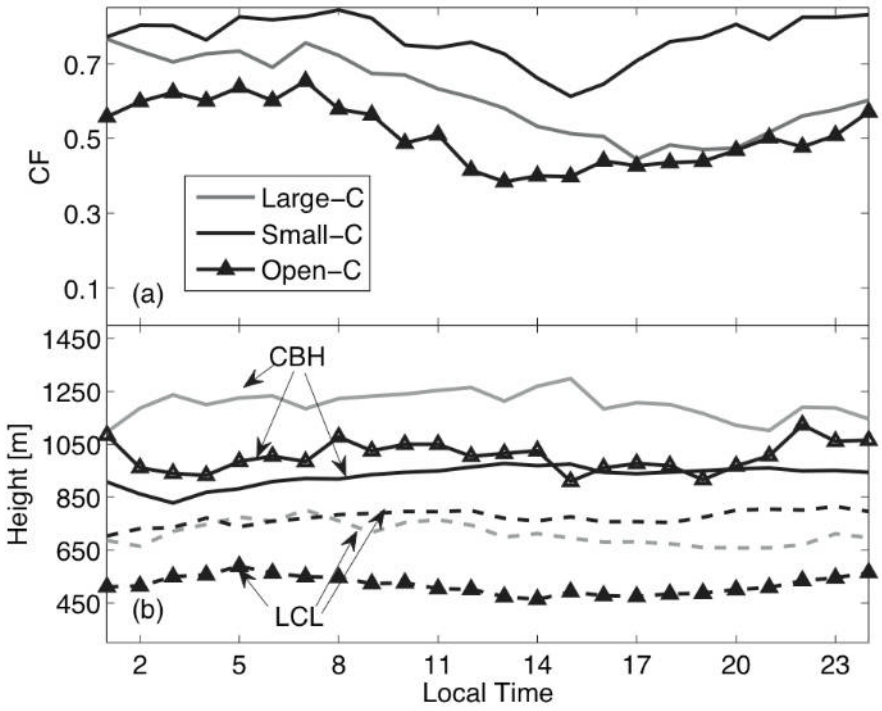

FIG. 9. Mean diurnal cycles of ceilometer-derived for large closed-cells (gray), small closed-cells (black line) and open cells (triangles), 2003 a) low-cloud frequency (CF) and LWP, b) cloud-base height (CBH, solid line) and lifting condensation levels (LCL, dashed lines).

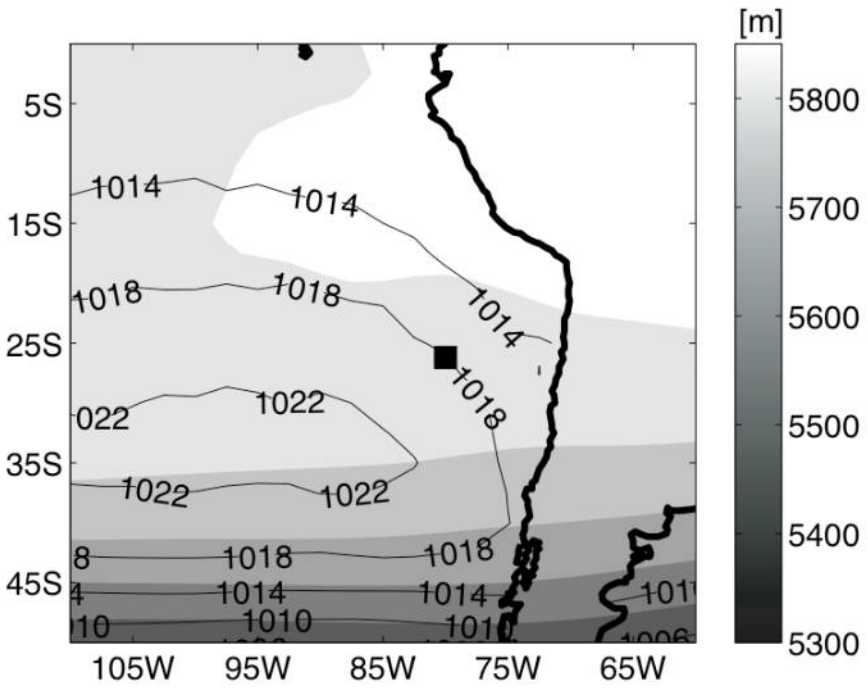

FIG. 10. Large closed cell composite. Contours indicate SLP and shades geopotential height at 500 hPa. The thick square represents the location of SFI.

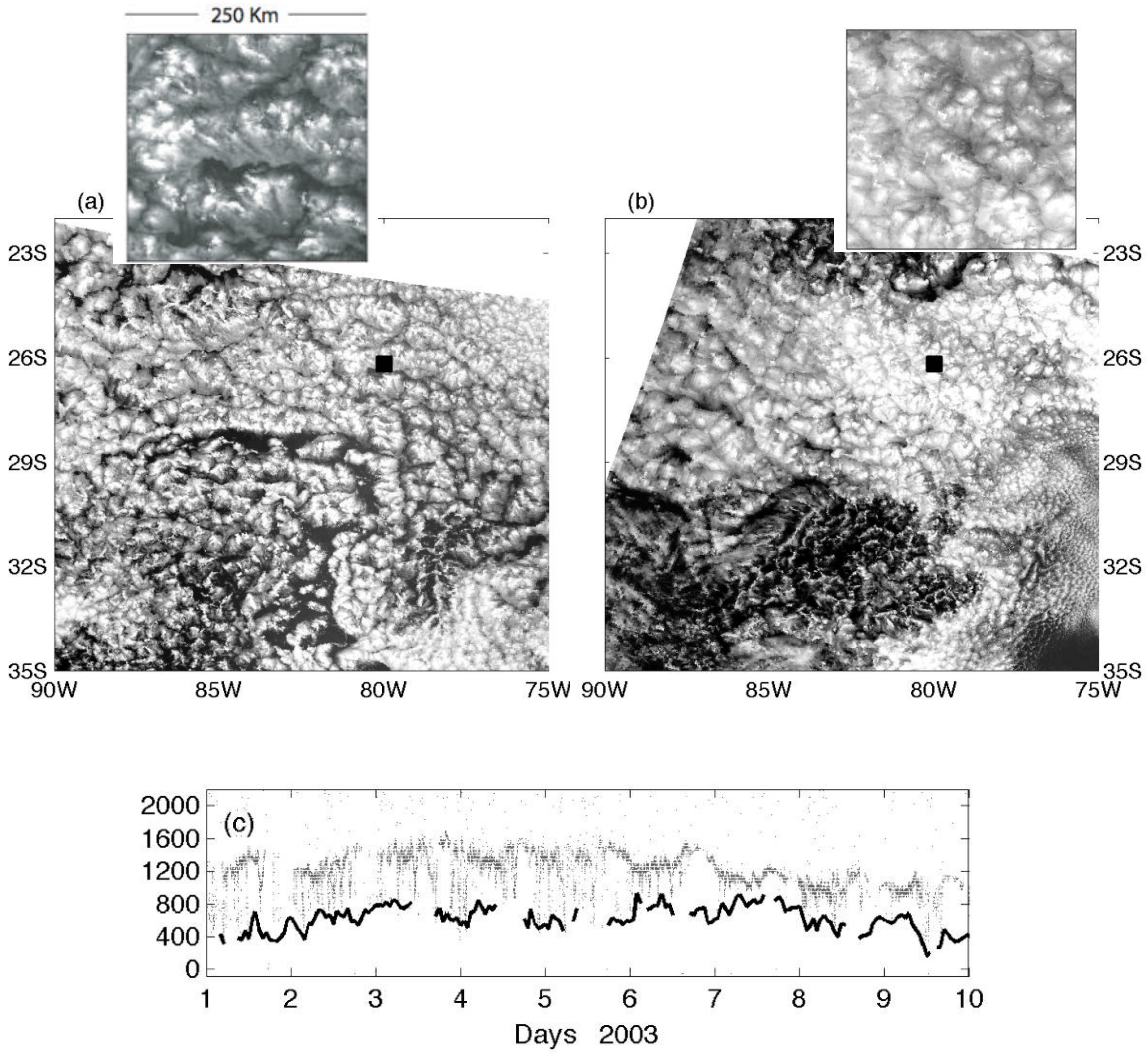

FIG. 11. An example of a period with large closed cell patterns: a) day 2 (Jan 2), b) day 6, with their correspondent enlargement around SFI (260Km by 260 Km area). The thick square represents the location of SFI. c) ceilometer cloud bases and LCL (black line) estimated from SST and moisture.

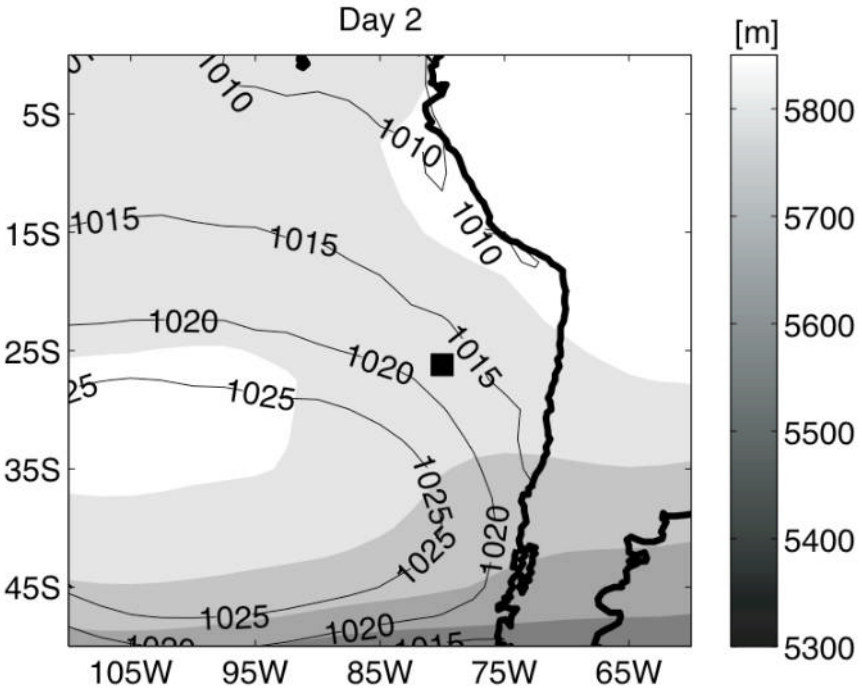

FIG. 12. Sea level pressure (contours) and geopotential height at 500 hPa (shaded) for day 2.

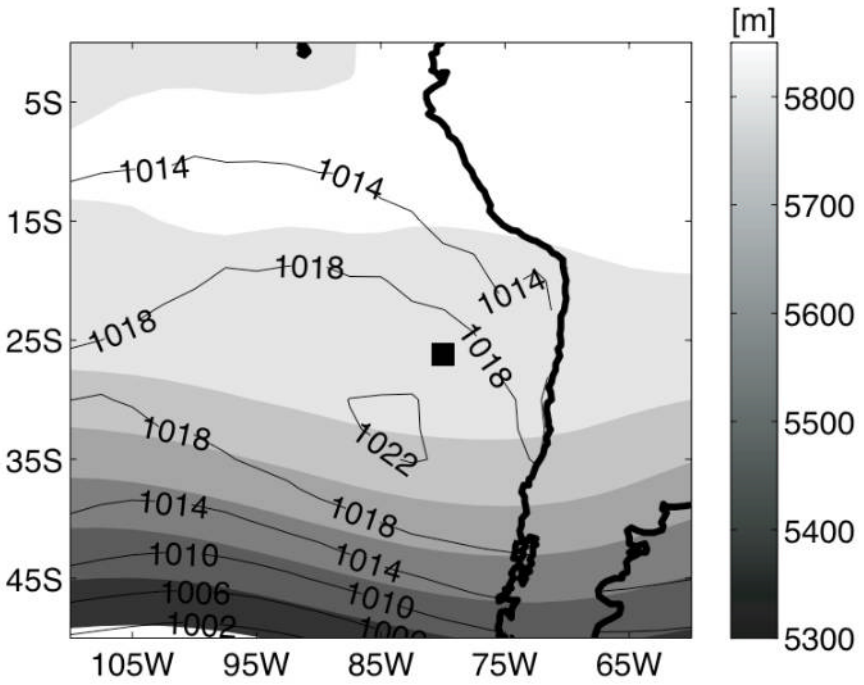

FIG. 13. Small closed cell composite. Contours indicate SLP and shades geopotential height at 500 hPa. The thick square represents the location of SFI.

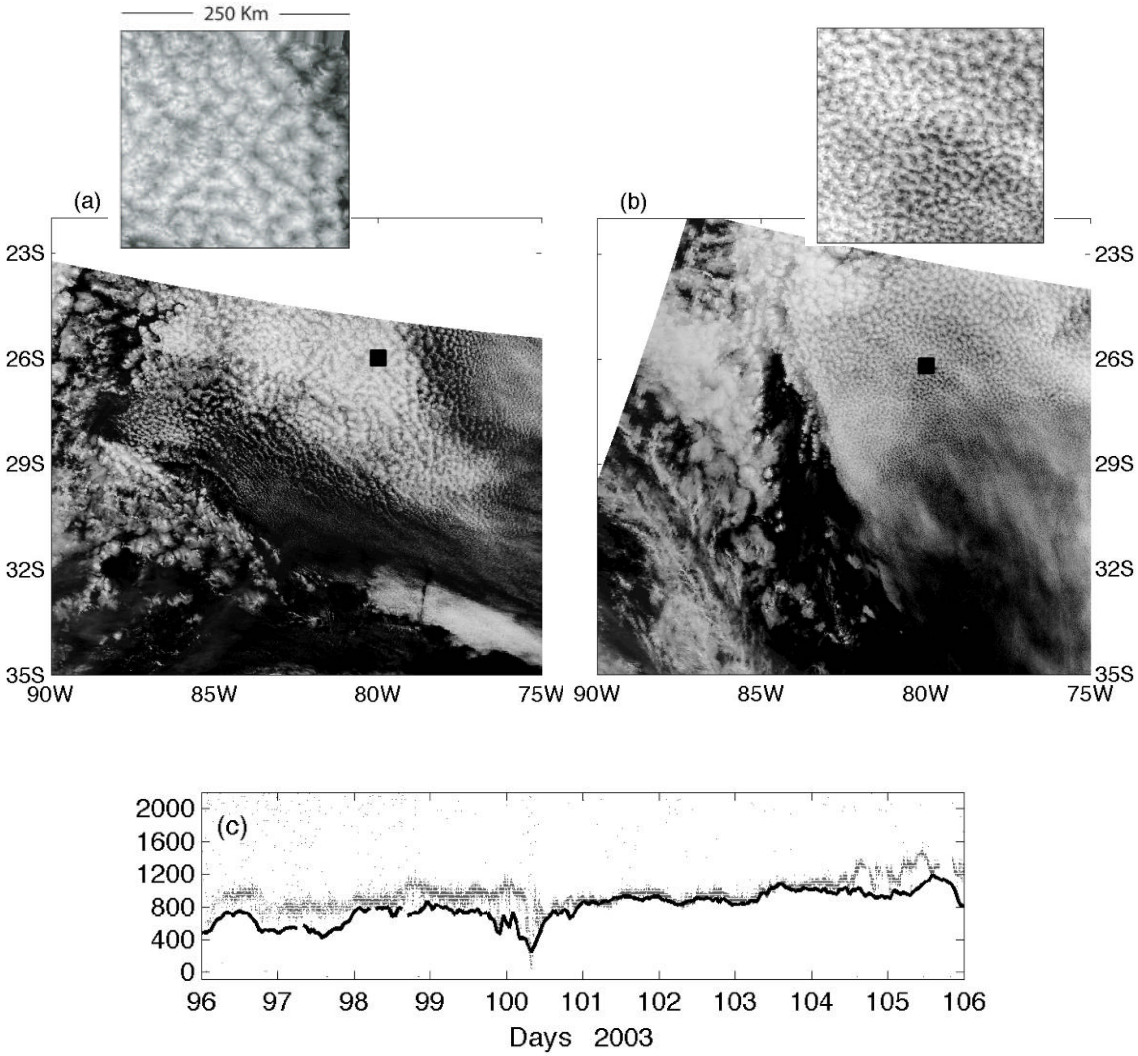

FIG. 14. As in FIG. 11 but for a small closed cell period: a) day 98 (April 8), b) day 102 and c) ceilometer cloud bases and LCL (black line).

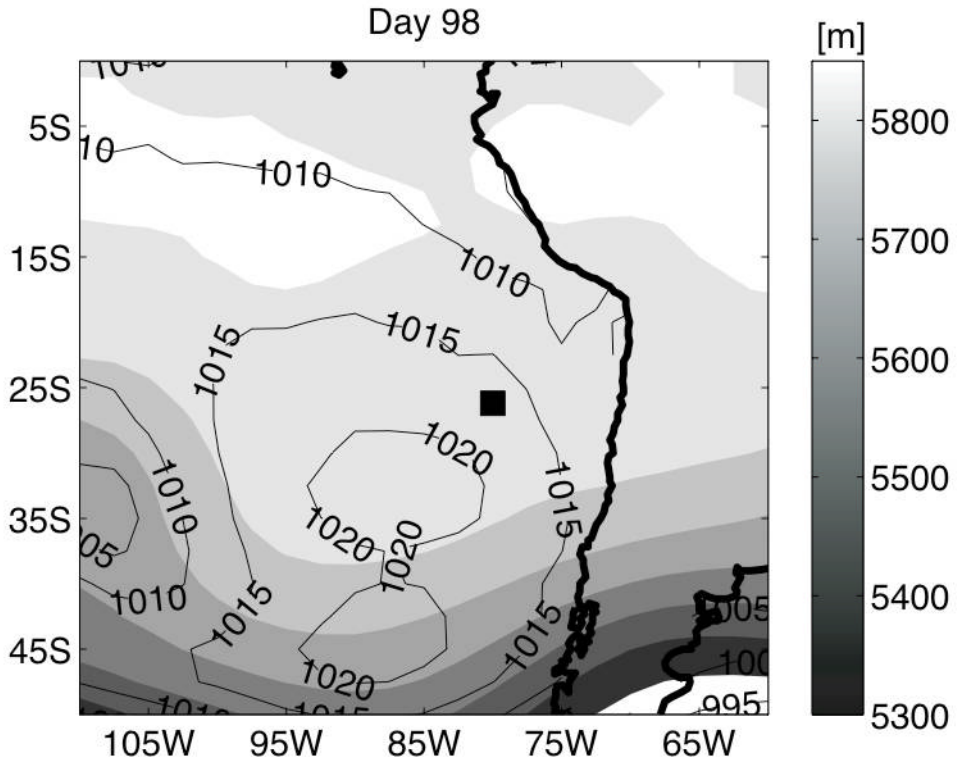

FIG. 15. As in FIG. 12 but for day 98.

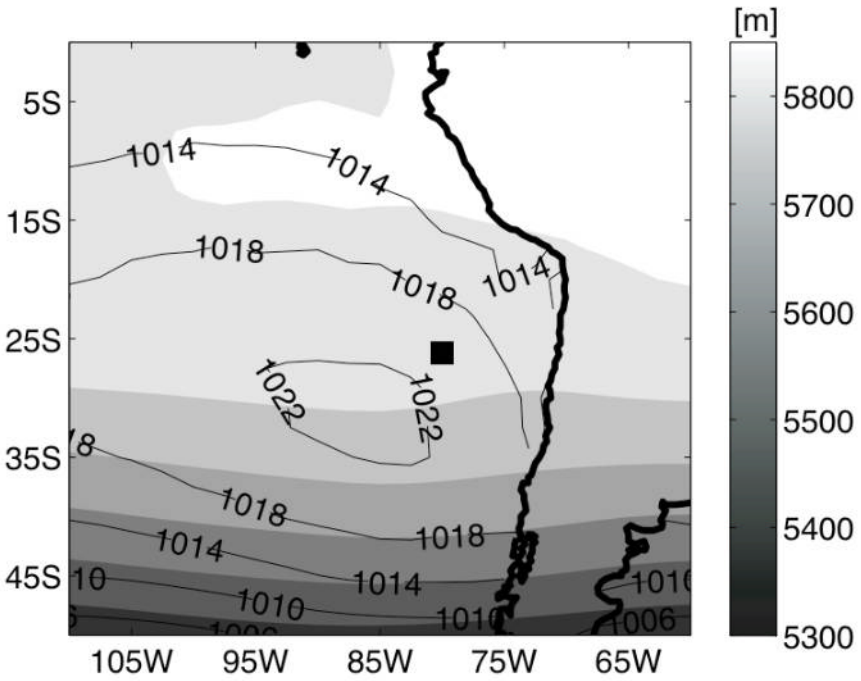

FIG. 16. Open cell composite. Contours indicate SLP and shades geopotential height at 500 hPa. The thick square represents the location of SFI.

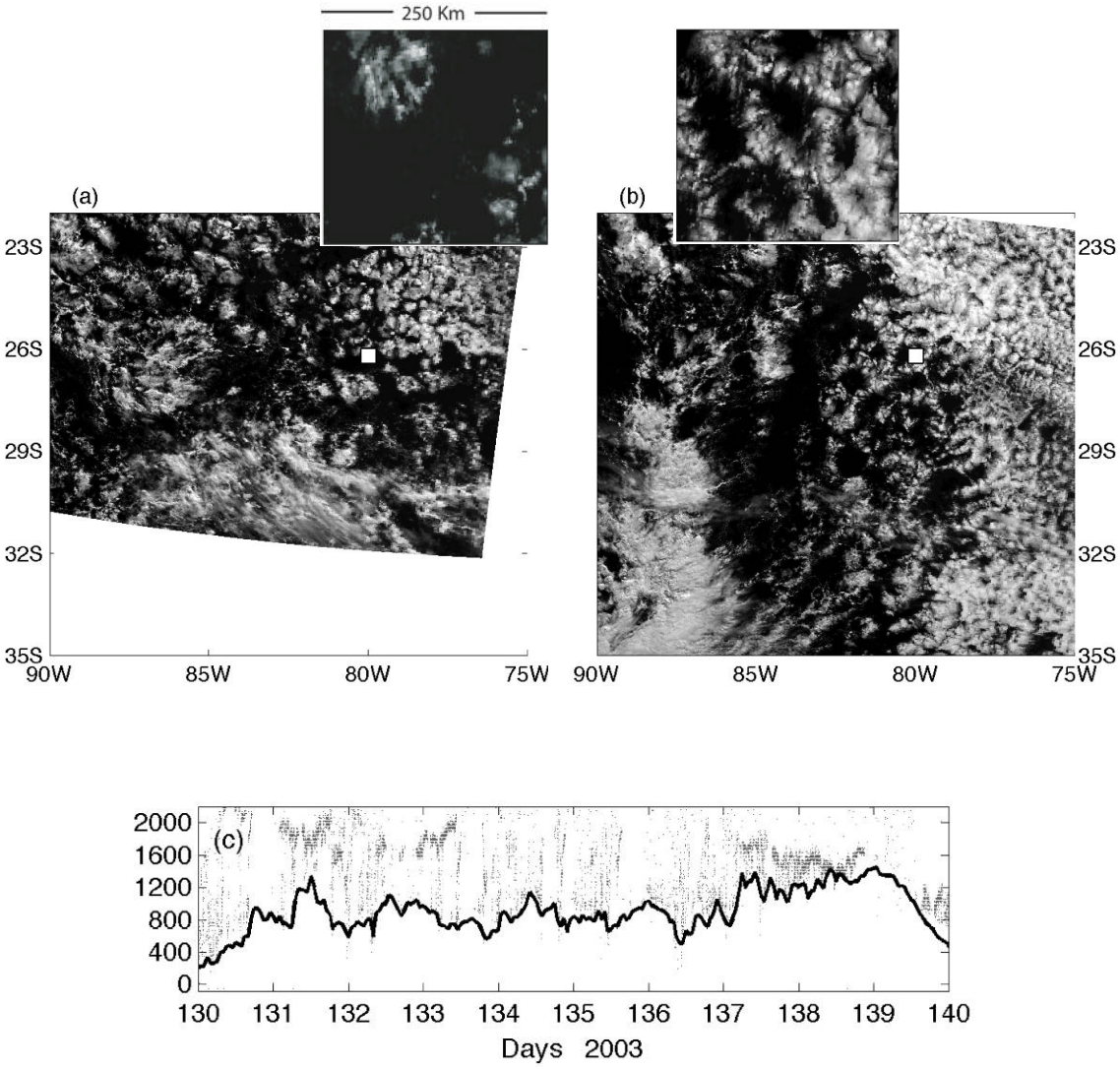

FIG. 17. As in FIG. 11 but for a open-cell like period: a) day 135 (May 15), b) day 137 and c) ceilometer cloud bases and LCL (black line).

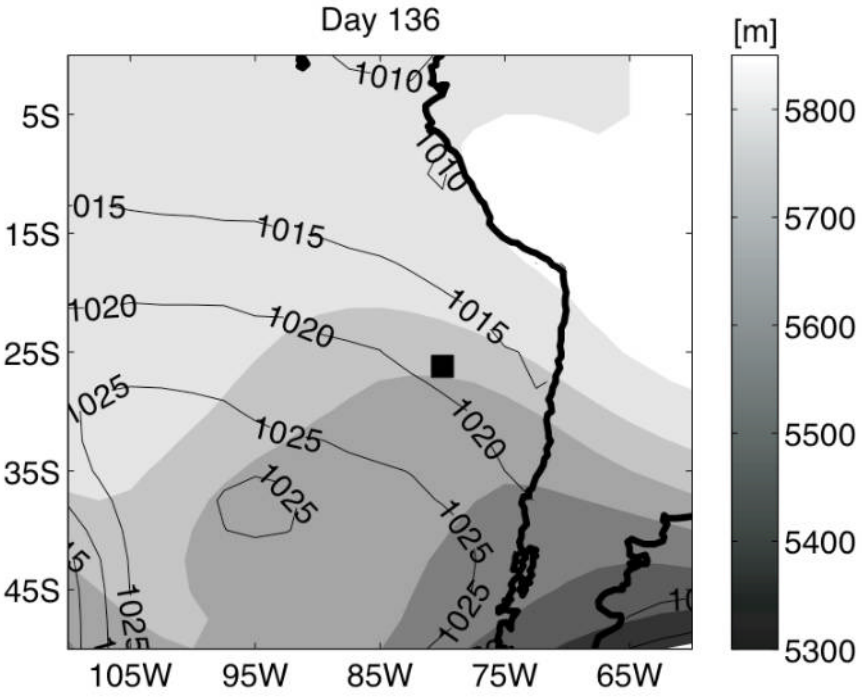

FIG. 18. As in FIG. 12 but for day 136.